Chinese Journal of Aeronautics, (2014),27(3): 634–642

Chinese Society of Aeronautics and Astronautics
& Beihang University

Chinese Journal of Aeronautics

cja@buaa.edu.cn
www.sciencedirect.com

Backstepping design of missile guidance and control based on adaptive fuzzy sliding mode control

Ran Maopeng [a], **Wang Qing** [a,*], **Hou Delong** [a], **Dong Chaoyang** [b]

[a] *School of Automation Science and Electrical Engineering, Beihang University, Beijing 100191, China*
[b] *School of Aeronautic Science and Engineering, Beihang University, Beijing 100191, China*

Received 3 June 2013; revised 15 July 2013; accepted 27 August 2013
Available online 24 April 2014

KEYWORDS

Adaptive fuzzy system;
Backstepping;
Integrated guidance and control;
Nonlinear;
Sliding mode control

Abstract This paper presents an integrated missile guidance and control law based on adaptive fuzzy sliding mode control. The integrated model is formulated as a block-strict-feedback nonlinear system, in which modeling errors, unmodeled nonlinearities, target maneuvers, etc. are viewed as unknown uncertainties. The adaptive nonlinear control law is designed based on backstepping and sliding mode control techniques. An adaptive fuzzy system is adopted to approximate the coupling nonlinear functions of the system, and for the uncertainties, we utilize an online-adaptive control law to estimate the unknown parameters. The stability analysis of the closed-loop system is also conducted. Simulation results show that, with the application of the adaptive fuzzy sliding mode control, small miss distances and smooth missile trajectories are achieved, and the system is robust against system uncertainties and external disturbances.

1. Introduction

Missile guidance and control systems are usually designed separately due to the assumption that there is a spectral separation between the guidance loop and the control loop. Based on this paradigm, a number of past missile systems which guarantee outstanding performance have been designed. However, it can be argued that this design paradigm cannot fully exploit synergistic relationships between the two subsystems or strictly maintain the stability of the overall system.[1] On the other hand, the spectral separation assumption may be invalid, especially at the end-game phase of the interception.[2] Integrated guidance and control (IGC) design was first put forward in Ref.[3], and has received much attention in recent years.[4–8] It was shown that IGC designs have the potential to enhance missile performance by viewing the two subsystems as an integrated system and accounting for the coupling between guidance and control dynamics.

Various control methods have been adopted in IGC designs. A small-gain theorem based IGC law was designed in Ref.[1] for missiles steered by both canard and tail controls, and the stability of the overall system could be guaranteed without the assumption that the angle between line-of-sight (LOS) and missile velocity was almost invariable. An IGC law based on adaptive output feedback and backstepping techniques was designed in Ref.[7] for formation flight, which was translated into better transient and steady-state range tracking performance. An IGC law based on the state-dependent

* Corresponding author. Tel.: +86 10 82338161.
E-mail address: wangqing@buaa.edu.cn (Q. Wang).

Peer review under responsibility of Editorial Committe of CJA.

Production and hosting by Elsevier

1000-9361 © 2014 Production and hosting by Elsevier Ltd. on behalf of CSAA & BUAA.
http://dx.doi.org/10.1016/j.cja.2014.04.007

Riccati equation approach for a moving-mass-actuated missile was designed in Ref.[8], and miss distances which were much less than the diameter of the missile were achieved. The nonlinear optimal control technique, the θ–D method, was employed in Ref.[9] to design an IGC law, and the controller did not require online computation of the state-dependent Riccati equation.

Sliding mode control (SMC) is another typical method in IGC designs. SMC is known to be an efficient control technique applicable to a wide class of nonlinear systems, due to its insensitivity to model uncertainties and external disturbances after reaching the sliding phase. SMC has been addressed in some previous studies for IGC designs.[2,10–14] Koren et al.[2] chose the zero-effort miss distance as the sliding variable. A robust SMC controller was then designed to deal with both system uncertainties and the difference between nonlinear and linear design methods. Shima et al.[10] defined the same sliding surface as that in Ref.[2]. Based on their approach, small distances could be achieved even in stringent interception scenarios. Hou and Duan[11] proposed an IGC scheme for homing missiles against ground fixed targets, and an SMC-based adaptive nonlinear control law was designed to guarantee a missile hit a target accurately with a desired impact attitude angle. Based on the assumption that each of the three channels of an IGC model can be independently designed, Yamasaki et al.[12] introduced an IGC design approach for a path-following uninhabited aerial vehicle. Dong et al.[13] developed a robust higher-order sliding mode (HOSM) based IGC law, in which the IGC design problem was considered to be equal to the stabilization of a third integral chain system. Zhao et al.[14] proposed a SMC-based nonlinear IGC strategy which took the higher-order dynamics of the system into account.

Although SMC has been widely applied to IGC designs, some problems still exist. Nearly all existing approaches are based on the assumption that the nonlinear functions in an IGC model could be accurately obtained. In practice, such an assumption may not be always guaranteed. In this paper, an IGC law based on adaptive fuzzy sliding mode control is firstly presented. The developed approach, when compared with the existing results, is novel in that the IGC law can guarantee high performance without the assumption that the coupling nonlinear functions in the integrated model can be accurately obtained.

2. Model derivation

2.1. Engagement kinematics

The planar engagement geometry is depicted in Fig. 1, where OXY is a Cartesian inertial reference frame, and M and T represent the missile and the target, respectively. The corresponding equations of motion between the missile and the target are as follows:[1]

$$\dot{R} = V_{\mathrm{T}}\cos(q-\theta_{\mathrm{T}}) - V_{\mathrm{M}}\cos(q-\theta_{\mathrm{M}}) \tag{1a}$$

$$R\dot{q} = -V_{\mathrm{T}}\sin(q-\theta_{\mathrm{T}}) + V_{\mathrm{M}}\sin(q-\theta_{\mathrm{M}}) \tag{1b}$$

where R is the relative range, q is the LOS angle, θ_{M} and θ_{T} are the missile and target flight path angles, respectively, and V_{M} and V_{T} are the missile and target velocities, respectively. Differentiating Eq. (1b) followed by the substitution of Eq. (1a), we get

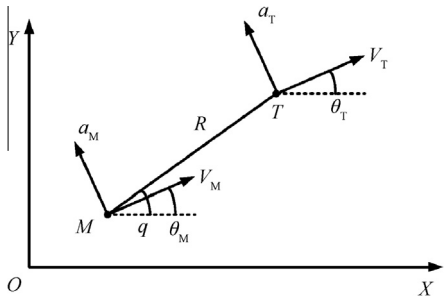

Fig. 1 Planar engagement geometry.

$$R\ddot{q} + 2\dot{R}\dot{q} = -\dot{V}_{\mathrm{T}}\sin(q-\theta_{\mathrm{T}}) + \dot{V}_{\mathrm{M}}\sin(q-\theta_{\mathrm{M}}) + V_{\mathrm{T}}\dot{\theta}_{\mathrm{T}} \times \cos(q-\theta_{\mathrm{T}}) - V_{\mathrm{M}}\dot{\theta}_{\mathrm{M}}\cos(q-\theta_{\mathrm{M}}) \tag{2}$$

Assume that $\dot{V}_{\mathrm{M}} = \dot{V}_{\mathrm{T}} = 0$, and define $V_q = R\dot{q}$, $a_{\mathrm{T}} = V_{\mathrm{T}}\dot{\theta}_{\mathrm{T}}$, and $a_{\mathrm{M}} = V_{\mathrm{M}}\dot{\theta}_{\mathrm{M}}$. Eq. (2) can be rewritten as

$$\dot{V}_q = -\frac{\dot{R}}{R}V_q + a_{\mathrm{T}}\cos(q-\theta_{\mathrm{T}}) - a_{\mathrm{M}}\cos(q-\theta_{\mathrm{M}}) \tag{3}$$

where a_{M} and a_{T} are the missile and target accelerations, respectively.

2.2. Missile dynamics

The planar missile dynamics are given by[15]

$$\dot{\alpha} = \frac{1}{mV_{\mathrm{M}}}(-T_{\mathrm{M}}\sin\alpha - L + mg\cos\theta_{\mathrm{M}}) + \omega_z \tag{4}$$

$$J_z\dot{\omega}_z = M_0 + M_{\delta_z}\delta_z \tag{5}$$

$$\dot{\vartheta} = \omega_z \tag{6}$$

$$\alpha = \vartheta - \theta_{\mathrm{M}} \tag{7}$$

where α is the angle of attack, m is the missile mass, T_{M} is the thrust of the missile, L is the lift force, ω_z is the pitch rate, J_z is the moment of inertia about z-axis, δ_z is the deflection angle for pitch control, ϑ is the pitch angle, M_{δ_z} is the control contribution to the angular acceleration, and $M_0 = M_0(\alpha, Ma, h, V_{\mathrm{M}}, \omega_z)$ represents the angular acceleration contributions from all other sources such as the angle of attack α, the Mach number Ma, the height h, and so on. M_0 is often approximated as follows:[16]

$$M_0 = M_\alpha\alpha + M_{\omega_z}\omega_z \tag{8}$$

where M_α and M_{ω_z} are the angular acceleration contributions from the angle of attack and pitch rate, respectively.

The lift force (L) and relative parameters ($M_\alpha, M_{\omega_z}, M_{\delta_z}$) are as follows:

$$\begin{cases} L = 57.3Qs\left(c_y^\alpha\alpha + c_y^{\delta_z}\delta_z\right) \\ M_\alpha = 57.3Qslm_z^\alpha\alpha \\ M_{\omega_z} = \dfrac{Qsl^2m_z^{\omega_z}}{V_{\mathrm{M}}} \\ M_{\delta_z} = 57.3Qslm_z^{\delta_z} \end{cases} \tag{9}$$

where Q is the dynamic pressure, s is the aerodynamic reference area, l is the reference length, c_y^α and $c_y^{\delta_z}$ are the lift force derivatives with respect to α and δ_z, respectively, and $m_z^\alpha, m_z^{\omega_z}$, and $m_z^{\delta_z}$ are the pitch moment derivatives with respect to α, ω_z, and δ_z, respectively.

2.3. Integrated model

According to the above analysis and with the assumption that during the end-game the missile has no thrust and the drag force is negligible, the integrated model can be written as

$$\begin{cases} \dot{V}_q = -\dfrac{\dot{R}}{R}V_q + \dfrac{-57.3Qsc_y^{\alpha}}{m}\alpha + g\cos\theta_{\mathrm{M}} + d_{V_q} \\ \dot{\alpha} = -\dfrac{57.3Qsc_y^{\alpha}}{mV_{\mathrm{M}}}\alpha + \dfrac{g\cos\theta_{\mathrm{M}}}{V_{\mathrm{M}}} + \omega_z + d_{\alpha} \\ \dot{\omega}_z = \dfrac{57.3Qslm_z^{\alpha}}{J_z}\alpha + \dfrac{57.3Qsl^2m_z^{\omega_z}}{J_zV_{\mathrm{M}}}\omega_z \\ \quad + \dfrac{57.3Qslm_z^{\delta_z}}{J_z}\delta_z + d_{\omega_z} \end{cases} \tag{10}$$

where d_{V_q}, d_{α}, and d_{ω_z} are the unknown bounded uncertainties (modeling errors caused by the assumptions, unmodeled nonlinearities, target maneuvers, etc.).

Define $x_1 = \dfrac{V_q}{-57.3Qsc_y^{\alpha}/m}$, $x_2 = \alpha$, $x_3 = \omega_z$, $u = \delta_z$, and $b = \dfrac{57.3Qslm_z^{\delta_z}}{J_z}$. The integrated model can be rewritten into

$$\begin{cases} \dot{x}_1 = f_1(x_1) + x_2 + d_1 \\ \dot{x}_2 = f_2(x_2) + x_3 + d_2 \\ \dot{x}_3 = f_3(x_2, x_3) + bu + d_3 \end{cases} \tag{11}$$

where

$$\begin{cases} f_1(x_1) = -\dfrac{\dot{R}}{R}x_1 + \dfrac{g\cos\theta_{\mathrm{M}}\cos(q-\theta_{\mathrm{M}})}{-57.3Qsc_y^{\alpha}/m} \\ f_2(x_2) = \dfrac{-57.3Qsc_y^{\alpha}}{mV_{\mathrm{M}}}x_2 + \dfrac{g\cos\theta_{\mathrm{M}}}{V_{\mathrm{M}}} \\ f_3(x_2, x_3) = \dfrac{57.3Qslm_z^{\alpha}}{J_z}x_2 + \dfrac{Qsl^2m_z^{\omega_z}}{J_zV_{\mathrm{M}}}x_3 \\ d_1 = \dfrac{d_{V_q}}{-57.3Qsc_y^{\alpha}/m}, \ d_2 = d_{\alpha} \\ d_3 = d_{\omega_z}, |d_i| \leqslant d_{i,\max} \ (i = 1,2,3) \end{cases}$$

With simplicity consideration, the IGC model (11) is in a strict-feedback form,[17] and the backstepping technique is suitable for dealing with such cascade systems. Moreover, SMC is known to be an efficient control technique to overcome model uncertainties. The main observation, in this paper, is to combine these two techniques to design a high-performance IGC law.

3. IGC law design

The task of the IGC law design is to find a suitable control u to make sure the missile hit the target, and during the process the missile attitude is stable. The IGC law design procedure in this paper is divided into three steps.

Step 1. Based on the intuition that zeroing $\dot{q}$ will lead to interception, we choose the first sliding surface as

$$s_1 = x_1 \tag{12}$$

The time derivative of s_1 is

$$\dot{s}_1 = \dot{x}_1 = f_1(x_1) + x_2 + d_1 \tag{13}$$

In the control system, we cannot measure the exact value of the nonlinear function $f_1(x_1)$, so it will be replaced by its estimated value $\hat{f}_1(x_1)$. Due to the universal approximation ability of an adaptive fuzzy system, it will be used here to approximate the uncertain nonlinear function $f_1(x_1)$. For a continuous function $f(\boldsymbol{x})$ defined in a close set $\boldsymbol{U}$ and any precision ε, there must exist a fuzzy logic system $F(\boldsymbol{x})$ that satisfies[18,19]

$$\sup_{\boldsymbol{x}\in\boldsymbol{U}}|F(\boldsymbol{x}) - f(\boldsymbol{x})| < \varepsilon \tag{14}$$

where $F(\boldsymbol{x})$ is composed of product inference, singleton fuzzification, center-average defuzzification, and Gauss membership functions.

(1) Product inference

$$\mu_f^l(\bar{y}^l) = \mu_{f_1^l}(x_1)\mu_{f_2^l}(x_2)\cdots\mu_{f_n^l}(x_n) \tag{15}$$

where $\boldsymbol{x} = [x_1, x_2, \ldots, x_n]^{\mathrm{T}}$ and $\bar{y}^l$ are the fuzzy logic system's input and output, respectively. Fuzzy sets f and $f_i^l (i = 1, 2, \ldots, n)$ are associated with the fuzzy membership functions $\mu_f^l(\bar{y}^l)$ and $\mu_{f_i^l}(x_i)$ $(i = 1, 2, \ldots, n)$, respectively.

(2) Singleton fuzzification

The rules to map a crisp point $\boldsymbol{x} = [x_1, x_2, \ldots, x_n]^{\mathrm{T}} \in \boldsymbol{U}$ into a fuzzy set $A_{\boldsymbol{x}}$ in $\boldsymbol{U}$ are: $A_{\boldsymbol{x}}$ is a fuzzy singleton with support $\underline{\boldsymbol{x}}$, i.e., $\mu_A(\underline{\boldsymbol{x}}') = 1$ for $\underline{\boldsymbol{x}}' = \underline{\boldsymbol{x}}$ and $\mu_A(\underline{\boldsymbol{x}}) = 0$ for all other $\underline{\boldsymbol{x}}' \in \boldsymbol{U}$ with $\underline{\boldsymbol{x}}' \neq \underline{\boldsymbol{x}}$.

(3) Center-average defuzzification

$$y = \frac{\sum_{l=1}^{r}\bar{y}^l \cdot \mu_f^l(\bar{y}^l)}{\sum_{l=1}^{r}\mu_f^l(\bar{y}^l)} \tag{16}$$

(4) Gauss membership function

$$\mu_{f_i^l}(x_i) = \exp\left[-\left(\frac{x_i - \bar{x}_i^l}{\sigma_i^l}\right)^2\right] \tag{17}$$

where $\bar{x}_i^l$ is the center of the Gauss curve and σ_i^l is the width of the Gauss curve.

By defining the fuzzy base function as

$$P_j(\boldsymbol{x}) = \frac{\prod_{i=1}^{n}\mu_{f_i^l}(x_i)}{\sum_{j=1}^{m}\left(\prod_{i=1}^{n}\mu_{f_i^l}(x_i)\right)} \quad (j = 1, 2, \ldots, m) \tag{18}$$

the fuzzy system can be written into the following equivalent form:

$$f(\boldsymbol{x}) = \frac{\sum_{j=1}^{m}\bar{y}^j\left(\prod_{i=1}^{n}\mu_{f_i^l}(x_i)\right)}{\sum_{j=1}^{m}\left(\prod_{i=1}^{n}\mu_{f_i^l}(x_i)\right)} = \boldsymbol{\theta}^{\mathrm{T}}\boldsymbol{P}(\boldsymbol{x}) \tag{19}$$

where $\boldsymbol{\theta} = [\bar{y}^1, \bar{y}^2, \ldots, \bar{y}^m]^{\mathrm{T}}$, $\boldsymbol{P}(\boldsymbol{x}) = [P_1(\boldsymbol{x}), P_2(\boldsymbol{x}), \ldots, P_m(\boldsymbol{x})]^{\mathrm{T}}$.

Details about this kind of adaptive fuzzy systems can be found in Refs.[18,19]. In this paper, we only need to construct the approximate Gauss membership functions of the system states. In practice, the membership functions will be determined by an iterative procedure according to the computational results.

Assuming an adaptive fuzzy system

$$f(\boldsymbol{x}) = \boldsymbol{\theta}_f^{\mathrm{T}}\boldsymbol{P}_f(\boldsymbol{x}) \tag{20}$$

where $\boldsymbol{\theta}_f$ is an unknown weight vector that needs online regulation and $\boldsymbol{P}_f(\boldsymbol{x})$ is a Gauss function as well as a fuzzy base function.

During the approximation process, we can get the optimum value

$$f^*(\boldsymbol{x}) = \boldsymbol{\theta}_f^{*\mathrm{T}} \boldsymbol{P}_f(\boldsymbol{x}) \tag{21}$$

where $\boldsymbol{\theta}_f^*$ is the optimum weight vector defined as

$$\boldsymbol{\theta}_f^* = \arg\min \left[\sup_{x \in U} |\hat{f}(\boldsymbol{x}) - f(\boldsymbol{x})| \right] \tag{22}$$

where $\hat{f}$ is the estimate of f. Note that we will use the corresponding hat "^" to denote the estimate value henceforth.

As shown in Eq. (14), there exists an approximation error ε_f that satisfies

$$f(\boldsymbol{x}) = f^*(\boldsymbol{x}) + \varepsilon_f \tag{23}$$

where $|\varepsilon_f| \leqslant \eta_f^*$, in which η_f^* is the upper boundary of the approximation error. However, the optimum parameter $\boldsymbol{\theta}_f^*$ is also substituted with the estimated value

$$\hat{f}(\boldsymbol{x}) = \hat{\boldsymbol{\theta}}_f^{\mathrm{T}} \boldsymbol{P}_f(\boldsymbol{x}) \tag{24}$$

From the above analysis, we have

$$f(\boldsymbol{x}) = f^*(\boldsymbol{x}) + \varepsilon_f = \hat{f}(\boldsymbol{x}) + \tilde{f}(\boldsymbol{x}) + \varepsilon_f = \hat{\boldsymbol{\theta}}_f^{\mathrm{T}} \boldsymbol{P}_f(\boldsymbol{x}) + \tilde{\boldsymbol{\theta}}_f^{\mathrm{T}} \boldsymbol{P}_f(\boldsymbol{x}) + \varepsilon_f \tag{25}$$

where $\tilde{f}(\boldsymbol{x}) = f^*(\boldsymbol{x}) - \hat{f}(\boldsymbol{x})$ and $\tilde{\boldsymbol{\theta}}_f = \boldsymbol{\theta}_f^* - \hat{\boldsymbol{\theta}}_f$ are the approximation error and the weight-value approximation error, respectively.

Therefore, with the result in Eq. (25), Eq. (13) can be rewritten as

$$\begin{aligned} \dot{s}_1 &= \hat{f}_1(x_1) + \tilde{f}_1(x_1) + \varepsilon_1 + x_2 + d_1 \\ &= \hat{\boldsymbol{\theta}}_1^{\mathrm{T}} \boldsymbol{P}_1(x_1) + \tilde{\boldsymbol{\theta}}_1^{\mathrm{T}} \boldsymbol{P}_1(x_1) + \varepsilon_1 + x_2 + d_1 \end{aligned} \tag{26}$$

We treat x_2 as the virtual command, which can be designed as

$$x_{2\mathrm{c}} = -k_1 s_1 - \hat{\boldsymbol{\theta}}_1^{\mathrm{T}} \boldsymbol{P}_1(x_1) - \hat{\varepsilon}_1 \mathrm{sgn}(s_1) - \hat{d}_{1,\max} \mathrm{sgn}(s_1) \tag{27}$$

For the uncertain system parameters $\hat{\boldsymbol{\theta}}_1, \hat{\varepsilon}_1$, and $\hat{d}_{1,\max}$ are unknown, the following online-adaptive control law is proposed:

$$\begin{cases} \dot{\hat{\boldsymbol{\theta}}}_1 = \eta_1^1 s_1 \boldsymbol{P}_1(x_1) \\ \dot{\hat{\varepsilon}}_1 = \eta_2^1 |s_1| \\ \dot{\hat{d}}_{1,\max} = \eta_3^1 |s_1| \end{cases} \tag{28}$$

where $\eta_i^1 > 0$ $(i = 1, 2, 3)$.

Step 2. The second sliding surface is given as

$$s_2 = x_2 - x_{2\mathrm{c}} \tag{29}$$

The time derivative of s_2 is

$$\dot{s}_2 = \dot{x}_2 - \dot{x}_{2\mathrm{c}} = f_2(x_2) + x_3 + d_2 - \dot{x}_{2\mathrm{c}} \tag{30}$$

In this step, we choose x_3 as the virtual command, and the derivation steps are quite similar to those in Step 1. For the sake of brevity, we give $x_{3\mathrm{c}}$ directly:

$$\begin{aligned} x_{3\mathrm{c}} = &-s_1 - k_2 s_2 - \hat{\boldsymbol{\theta}}_2^{\mathrm{T}} \boldsymbol{P}_2(x_2, x_3) - \hat{\varepsilon}_2 \mathrm{sgn}(s_2) \\ &- \hat{d}_{2,\max} \mathrm{sgn}(s_2) + \dot{x}_{2\mathrm{c}} \end{aligned} \tag{31}$$

where

$$\begin{cases} \dot{\hat{\boldsymbol{\theta}}}_2 = \eta_1^2 s_2 \boldsymbol{P}_2(x_2) \\ \dot{\hat{\varepsilon}}_2 = \eta_2^2 |s_2| \\ \dot{\hat{d}}_{2,\max} = \eta_3^2 |s_2| \end{cases} \tag{32}$$

with $\eta_i^2 > 0$ $(i = 1, 2, 3)$.

In Eq. (31), $\dot{x}_{2\mathrm{c}}$ can be obtained from a first-order low-band filter. With the filter, the "computation explosion" problem in traditional backstepping designs can be avoided.[20]

Step 3. The third sliding surface is given as

$$s_3 = x_3 - x_{3\mathrm{c}} \tag{33}$$

The time derivative of s_3 is

$$\dot{s}_3 = \dot{x}_3 - \dot{x}_{3\mathrm{c}} = f_3(x_2, x_3) + bu + d_3 - \dot{x}_{3\mathrm{c}} \tag{34}$$

In this step, we obtain the actual control signal

$$\begin{aligned} u = &-\hat{b}^{-1}(s_2 + k_3 s_3 + \hat{\boldsymbol{\theta}}_3^{\mathrm{T}} \boldsymbol{P}_3(x_2, x_3) + \hat{\varepsilon}_3 \mathrm{sgn}(s_3) \\ &+ \hat{d}_{3,\max} \mathrm{sgn}(s_3) - \dot{x}_{3\mathrm{c}}) \end{aligned} \tag{35}$$

where

$$\begin{cases} \dot{\hat{\boldsymbol{\theta}}}_3 = \eta_1^3 s_3 \boldsymbol{P}_3(x_2, x_3) \\ \dot{\hat{\varepsilon}}_3 = \eta_2^3 |s_3| \\ \dot{\hat{d}}_{3,\max} = \eta_3^3 |s_3| \\ \dot{\hat{b}}^{-1} = \eta_4^3 s_3 \hat{b} u \end{cases} \tag{36}$$

with $\eta_i^3 > 0$ $(i = 1, 2, 3, 4)$.

Finally, we state the complete control law as follows:

$$\begin{cases} s_1 = x_1 \\ x_{2\mathrm{c}} = -k_1 s_1 - \hat{\boldsymbol{\theta}}_1^{\mathrm{T}} \boldsymbol{P}_1(x_1) - \hat{\varepsilon}_1 \mathrm{sgn}(s_1) - \hat{d}_{1,\max} \mathrm{sgn}(s_1) \\ s_2 = x_2 - x_{2\mathrm{c}} \\ x_{3\mathrm{c}} = -s_1 - k_2 s_2 - \hat{\boldsymbol{\theta}}_2^{\mathrm{T}} \boldsymbol{P}_2(x_2, x_3) - \hat{\varepsilon}_2 \mathrm{sgn}(s_2) \\ \qquad -\hat{d}_{2,\max} \mathrm{sgn}(s_2) + \dot{x}_{2\mathrm{c}} \\ s_3 = x_3 - x_{3\mathrm{c}} \\ u = -\hat{b}^{-1}(s_2 + k_3 s_3 + \hat{\boldsymbol{\theta}}_3^{\mathrm{T}} \boldsymbol{P}_3(x_2, x_3) + \hat{\varepsilon}_3 \mathrm{sgn}(s_3) \\ \qquad +\hat{d}_{3,\max} \mathrm{sgn}(s_3) - \dot{x}_{3\mathrm{c}}) \end{cases} \tag{37}$$

The online-adaptive laws of the unknown parameters are defined in Eqs. (28), (32), and (36).

4. Stability analysis

Define $\tilde{\boldsymbol{\theta}}_i = \boldsymbol{\theta}_i - \hat{\boldsymbol{\theta}}_i, \tilde{\varepsilon}_i = \varepsilon_i - \hat{\varepsilon}_i, \tilde{d}_{i,\max} = d_{i,\max} - \hat{d}_{i,\max}$ $(i = 1, 2, 3)$, and $\tilde{b}^{-1} = b^{-1} - \hat{b}^{-1}$. Substitute Eqs. (27) and (29) into Eq. (13), and get

$$\begin{aligned} \dot{s}_1 = &f_1(x_1) - k_1 s_1 - \hat{\boldsymbol{\theta}}_1^{\mathrm{T}} \boldsymbol{P}_1(x_1) - \hat{\varepsilon}_1 \mathrm{sgn}(s_1) - \hat{d}_{1,\max} \mathrm{sgn}(s_1) + d_1 \\ &+ s_2 = \tilde{\boldsymbol{\theta}}_1^{\mathrm{T}} P_1(x_1) + \varepsilon_1 - k_1 s_1 - \hat{\varepsilon}_1 \mathrm{sgn}(s_1) \\ &- \hat{d}_{1,\max} \mathrm{sgn}(s_1) + d_1 + s_2 \end{aligned} \tag{38}$$

Substitute Eqs. (31) and (33) into Eq. (30), and get

$$\begin{aligned} \dot{s}_2 = &f_2(x_2) - s_1 - k_2 s_2 - \hat{\boldsymbol{\theta}}_2^{\mathrm{T}} \boldsymbol{P}_2(x_2) - \hat{\varepsilon}_2 \mathrm{sgn}(s_2) - \hat{d}_{2,\max} \mathrm{sgn}(s_2) \\ &+ \dot{x}_{2\mathrm{c}} + d_2 - \dot{x}_{2\mathrm{c}} + s_3 = \tilde{\boldsymbol{\theta}}_2^{\mathrm{T}} \boldsymbol{P}_2(x_2) + \varepsilon_2 - s_1 - k_2 s_2 \\ &- \hat{\varepsilon}_2 \mathrm{sgn}(s_2) - \hat{d}_{2,\max} \mathrm{sgn}(s_2) + d_2 + s_3 \end{aligned} \tag{39}$$

Substitute Eq. (35) into Eq. (34), and get

$$\begin{aligned}\dot{s}_3 =& f_3(x_2,x_3) - b\hat{b}^{-1}(s_2 + k_3 s_3 + \hat{\boldsymbol{\theta}}_3^{\mathrm{T}}\boldsymbol{P}_3(x_2,x_3) + \hat{\varepsilon}_3\mathrm{sgn}(s_3) \\ &+ \hat{d}_{3,\max}\mathrm{sgn}(s_3) - \dot{x}_{3c}) + d_3 - \dot{x}_{3c} = f_3(x_2,x_3) \\ &- (s_2 + k_3 s_3 + \hat{\boldsymbol{\theta}}_3^{\mathrm{T}}\boldsymbol{P}_3(x_2,x_3) + \hat{\varepsilon}_3\mathrm{sgn}(s_3) + \hat{d}_{3,\max}\mathrm{sgn}(s_3) - \dot{x}_{3c}) \\ &+ b\tilde{b}^{-1}(s_2 + k_3 s_3 + \hat{\boldsymbol{\theta}}_3^{\mathrm{T}}\boldsymbol{P}_3(x_2,x_3) + \hat{\varepsilon}_3\mathrm{sgn}(s_3) + \hat{d}_{3,\max}\mathrm{sgn}(s_3) - \dot{x}_{3c}) \\ &+ d_3 - \dot{x}_{3c} = \varepsilon_3 + \tilde{\boldsymbol{\theta}}_3^{\mathrm{T}}\boldsymbol{P}_3(x_2,x_3) - s_2 - k_3 s_3 - \hat{\varepsilon}_3\mathrm{sgn}(s_3) \\ &- \hat{d}_{3,\max}\mathrm{sgn}(s_3) + b\tilde{b}^{-1}(s_2 + k_3 s_3 + \hat{\boldsymbol{\theta}}_3^{\mathrm{T}}\boldsymbol{P}_3(x_2,x_3) + \hat{\varepsilon}_3\mathrm{sgn}(s_3) \\ &+ \hat{d}_{3,\max}\mathrm{sgn}(s_3) - \dot{x}_{3c}) + d_3 = \varepsilon_3 + \tilde{\boldsymbol{\theta}}_3^{\mathrm{T}}\boldsymbol{P}_3(x_2,x_3) - s_2 \\ &- k_3 s_3 - \hat{\varepsilon}_3\mathrm{sgn}(s_3) - \hat{d}_{3,\max}\mathrm{sgn}(s_3) - b\tilde{b}^{-1}\hat{b}u + d_3 \end{aligned} \tag{40}$$

Theorem 1. *Considering the nonlinear system Eq. (11) with bounded uncertainties, if adaptive fuzzy systems are utilized to approximate the uncertain functions $f_1(x_1)$, $f_2(x_2)$, and $f_3(x_2, x_3)$, and in the SMC control law Eq. (37), the adaptive parameters are adjusted by the system online adaptive control laws shown in Eqs. (28), (32), and (36), then the system sliding modes are asymptotically accessible and the closed-loop system is asymptotically stable.*

Before the proof, we need the following lemma.

Lemma 1. [Babalat's Lemma] *If $f(t)$ is a uniformly continuous function and $\lim_{t\to\infty}\int_0^t f(\tau)\mathrm{d}\tau$ exists, then $f(t)$ converges to zero asymptotically.*

Proof of Theorem 1. Choose the quasi Lyapunov function as

$$\begin{aligned}V =& \frac{1}{2}\sum_{i=1}^{3} s_i^2 + \frac{1}{2}\sum_{i=1}^{3}\frac{1}{\eta_1^i}\tilde{\boldsymbol{\theta}}_i^{\mathrm{T}}\tilde{\boldsymbol{\theta}}_i + \frac{1}{2}\sum_{i=1}^{3}\frac{1}{\eta_2^i}\tilde{\varepsilon}_i^2 \\ &+ \frac{1}{2}\sum_{i=1}^{3}\frac{1}{\eta_3^i}\tilde{d}_{i,\max}^2 + \frac{|b|}{2\eta_4}(\tilde{b}^{-1})^2 \end{aligned} \tag{41}$$

Differentiate V along the track of the system (11), and obtain

$$\begin{aligned}\dot{V} =& \sum_{i=1}^{3} s_i\dot{s}_i + \sum_{i=1}^{3}\frac{1}{\eta_1^i}\tilde{\boldsymbol{\theta}}_i^{\mathrm{T}}\dot{\tilde{\boldsymbol{\theta}}}_i + \sum_{i=1}^{3}\frac{1}{\eta_2^i}\tilde{\varepsilon}_i\dot{\tilde{\varepsilon}}_i \\ &+ \sum_{i=1}^{3}\frac{1}{\eta_3^i}\tilde{d}_{i,\max}\dot{\tilde{d}}_{i,\max} - \frac{b}{\eta_4}\tilde{b}^{-1}\dot{\tilde{b}}^{-1} \end{aligned} \tag{42}$$

Substitute Eqs. (38)–(40) into Eq. (42), and get

$$\begin{aligned}\dot{V} =& s_1(\tilde{\boldsymbol{\theta}}_1^{\mathrm{T}}\boldsymbol{P}_1(x_1) + \varepsilon_1 - k_1 s_1 - \hat{\varepsilon}_1\mathrm{sgn}(s_1) - \hat{d}_{1,\max}\mathrm{sgn}(s_1) + d_1 + s_2) \\ &+ s_2\Big(\tilde{\boldsymbol{\theta}}_2^{\mathrm{T}}\boldsymbol{P}_2(x_2,x_3) + \varepsilon_2 - s_1 - k_2 s_2 - \hat{\varepsilon}_2\mathrm{sgn}(s_2) \\ &\quad - \hat{d}_{2,\max}\mathrm{sgn}(s_2) + d_2 + s_3\Big) \\ &+ s_3\Big(\tilde{\boldsymbol{\theta}}_3^{\mathrm{T}}\boldsymbol{P}_3(x_2,x_3) + \varepsilon_3 - s_2 - k_3 s_3 - \hat{\varepsilon}_3\mathrm{sgn}(s_3) \\ &\quad - \hat{d}_{3,\max}\mathrm{sgn}(s_3) + b\tilde{b}^{-1}\hat{b}u + d_3\Big) \\ &- \sum_{i=1}^{3}\frac{1}{\eta_1^i}\tilde{\boldsymbol{\theta}}_i^{\mathrm{T}}\dot{\hat{\boldsymbol{\theta}}}_i - \sum_{i=1}^{3}\frac{1}{\eta_2^i}\tilde{\varepsilon}_i\dot{\hat{\varepsilon}}_i - \sum_{i=1}^{3}\frac{1}{\eta_3^i}\tilde{d}_{i,\max}\dot{\hat{d}}_{i,\max} + \frac{b}{\eta_4}\tilde{b}^{-1}\dot{\tilde{b}}^{-1} \leqslant \\ &- k_1 s_1^2 + s_1\tilde{\boldsymbol{\theta}}_1^{\mathrm{T}}\boldsymbol{P}_1(x_1) + \varepsilon_1|s_1| - \hat{\varepsilon}_1|s_1| + d_{1,\max}|s_1| - \hat{d}_{1,\max}|s_1| \\ &- k_2 s_2^2 + s_2\tilde{\boldsymbol{\theta}}_2^{\mathrm{T}}\boldsymbol{P}_2(x_2,x_3) + \varepsilon_2|s_2| - \hat{\varepsilon}_2|s_2| + d_{2,\max}|s_2| - \hat{d}_{2,\max}|s_2| \\ &- k_3 s_3^2 + s_3\tilde{\boldsymbol{\theta}}_3^{\mathrm{T}}\boldsymbol{P}_3(x_2,x_3) + \varepsilon_3|s_3| - \hat{\varepsilon}_3|s_3| + d_{3,\max}|s_3| - \hat{d}_{3,\max}|s_3| \\ &- s_3 b\tilde{b}^{-1}\hat{b}u - \sum_{i=1}^{3}\frac{1}{\eta_1^i}\tilde{\boldsymbol{\theta}}_i^{\mathrm{T}}\dot{\hat{\boldsymbol{\theta}}}_i - \sum_{i=1}^{3}\frac{1}{\eta_2^i}\tilde{\varepsilon}_i\dot{\hat{\varepsilon}}_i - \sum_{i=1}^{3}\frac{1}{\eta_3^i}\tilde{d}_{i,\max}\dot{\hat{d}}_{i,\max} \\ &+ \frac{b}{\eta_4}\tilde{b}^{-1}\dot{\tilde{b}}^{-1} = -\sum_{i=1}^{3}k_i s_i^2 + \sum_{i=1}^{3}\tilde{\varepsilon}_i|s_i| + \sum_{i=1}^{3}\tilde{d}_{i,\max}|s_i| + s_1\tilde{\boldsymbol{\theta}}_1^{\mathrm{T}}\boldsymbol{P}_1(x_1) \\ &+ s_2\tilde{\boldsymbol{\theta}}_2^{\mathrm{T}}\boldsymbol{P}_2(x_2,x_3) + s_3\tilde{\boldsymbol{\theta}}_3^{\mathrm{T}}\boldsymbol{P}_3(x_2,x_3) - s_3 b\tilde{b}^{-1}\hat{b}u - \sum_{i=1}^{3}\frac{1}{\eta_1^i}\tilde{\boldsymbol{\theta}}_i^{\mathrm{T}}\dot{\hat{\boldsymbol{\theta}}}_i \\ &- \sum_{i=1}^{3}\frac{1}{\eta_2^i}\tilde{\varepsilon}_i\dot{\hat{\varepsilon}}_i - \sum_{i=1}^{3}\frac{1}{\eta_3^i}\tilde{d}_{i,\max}\dot{\hat{d}}_{i,\max} + \frac{b}{\eta_4}\tilde{b}^{-1}\dot{\tilde{b}}^{-1} = -\sum_{i=1}^{3}k_i s_i^2 \\ &+ \sum_{i=1}^{3}\tilde{\boldsymbol{\theta}}_i^{\mathrm{T}}\left(s_i P_i - \frac{1}{\eta_1^i}\dot{\hat{\boldsymbol{\theta}}}_i\right) + \sum_{i=1}^{3}\tilde{\varepsilon}_i\left(|s_i| - \frac{1}{\eta_2^i}\dot{\hat{\varepsilon}}_i\right) \\ &+ \sum_{i=1}^{3}d_{i,\max}\left(|s_i| - \frac{1}{\eta_3^i}\dot{\hat{d}}_{i,\max}\right) - b\tilde{b}^{-1}\left(s_3\hat{b}u - \frac{1}{\eta_4}\dot{\hat{b}}^{-1}\right) \end{aligned} \tag{43}$$

Associating with Eqs. (28), (32), and (36), we have

$$\dot{V} \leqslant -\sum_{i=1}^{3}k_i s_i^2 \leqslant 0 \tag{44}$$

Thus $s_i, \tilde{\theta}_i, \tilde{\varepsilon}_i, d_{i,\max}$ $(i = 1, 2, 3)$, and $\tilde{b}^{-1}$ are all bounded.

Define $k = \min\{k_1,k_2,k_3\}$ and $s = [s_1,s_2, s_3]^{\mathrm{T}}$. Eq. (44) can be rewritten as

$$\dot{V} \leqslant -k\|\boldsymbol{s}\|_2^2 \tag{45}$$

Integration of Eq. (40) from $t = 0$ to $t \to \infty$ reveals that

$$\int_0^\infty k\|\boldsymbol{s}(\tau)\|_2^2\mathrm{d}\tau \leqslant -\int_0^\infty \dot{V}(\tau)\mathrm{d}\tau = V(0) - V(\infty) < +\infty \tag{46}$$

Applying Lemma 1 to Eq. (43), we get that, while $t \to 0$, $\|\boldsymbol{s}\|_2^2 \to 0$, i.e., $s_i \to 0$ $(i = 1,2,3)$.

Therefore, it can be concluded that the system sliding modes are asymptotically accessible and the closed-loop system is asymptotically stable, and this completes the proof. □

5. Simulation results

This section presents simulation results of the proposed IGC law on a numerical example introduced in Ref.[21]. In this simulation study, the constant missile speed is assumed to be $V_{\mathrm{M}} = 3.5Ma$. The initial missile attitude and control fins are α (0) = 0° and $\delta_z(0)$ = 0°. The initial missile flight path angle is $\theta_{\mathrm{M}}(0)$ = 0°. The constant target speed is assumed to be $V_{\mathrm{T}} = 900$ m/s. The initial target flight path angle is $\theta_{\mathrm{T}}(0)$ = 10°. The initial missile position coordinate is (0,16) km. The initial target position coordinate is (1,16.4) km. The missile model parameters are as follows:

$$\frac{57.3Qsc_y^{\alpha}}{mV_{\mathrm{M}}} = 0.3487, \quad \frac{57.3Qsc_y^{\delta_z}}{mV_{\mathrm{M}}} = 0.068$$

$$\frac{57.3QSlm_z^{\alpha}}{J_z} = -17.801, \quad \frac{Qsl^2m_z^{\omega_z}}{J_zV_{\mathrm{M}}} = -0.2741$$

$$\frac{57.3Qslm_z^{\delta_z}}{J_z} = -31.267$$

The actuator dynamic is approximated as a first-order time delay system with a time constant of 0.01s, and the control surface deflection limit is $|\delta_z| \leqslant 30°$.

The controller parameters are given as $k_1 = 0.8$, $k_2 = 1.0$, $k_3 = 1.0$, $\hat{b}^{-1}(0) = -0.1$, $\hat{\boldsymbol{\theta}}_i(0) = [0,0,0]^{\mathrm{T}}$, $\hat{\varepsilon}_i(0) = 0$, and $\hat{d}_{i,\max}(0) = 0$ $(i = 1,2,3)$. Assuming that $|x_1| \leqslant 2\pi$, $|x_2| \leqslant \frac{\pi}{2}$, and $|x_3| \leqslant \pi$, we choose the fuzzy base functions as follows:

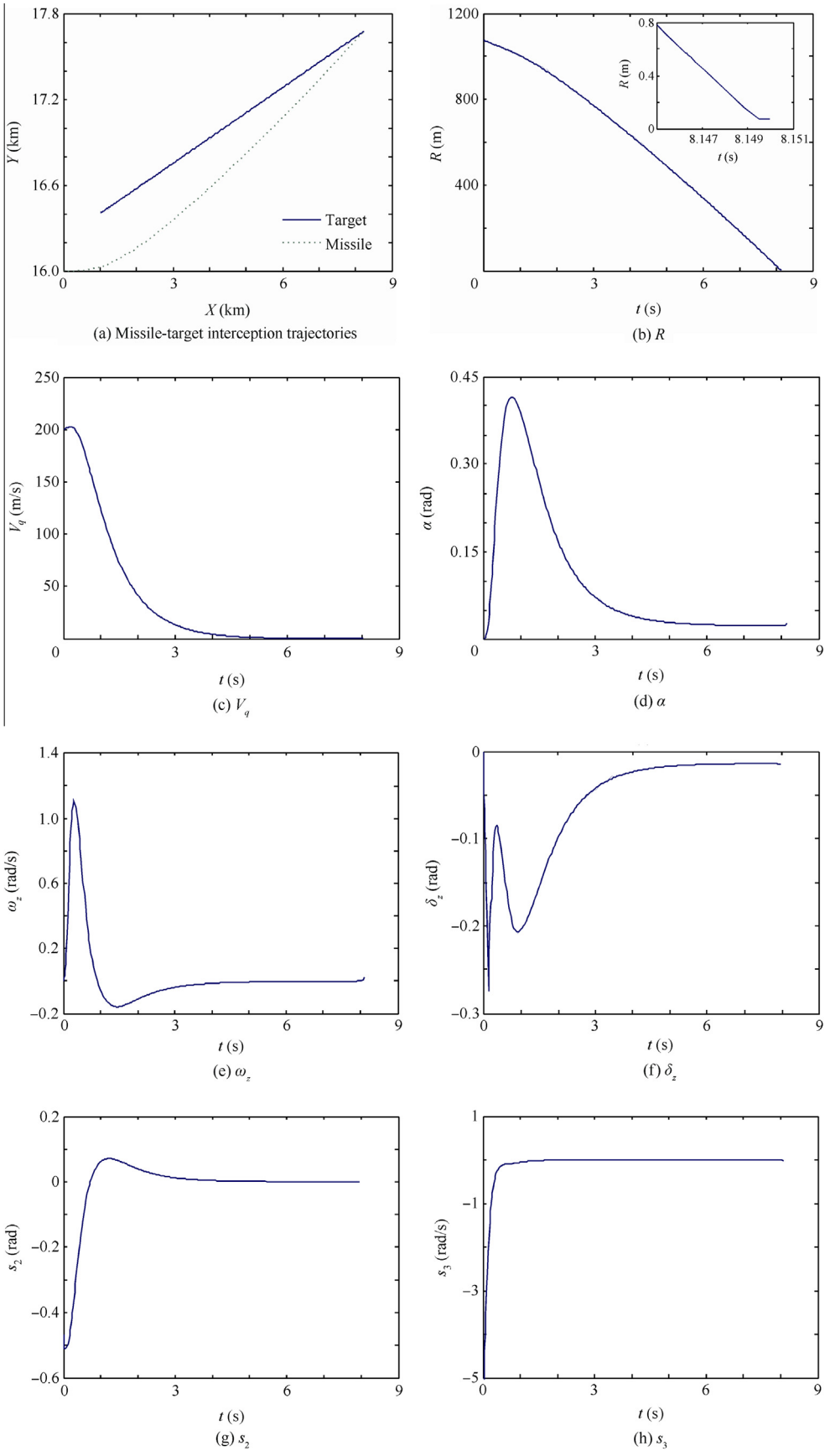

Fig. 2 Simulation results of the proposed IGC law in Case 1.

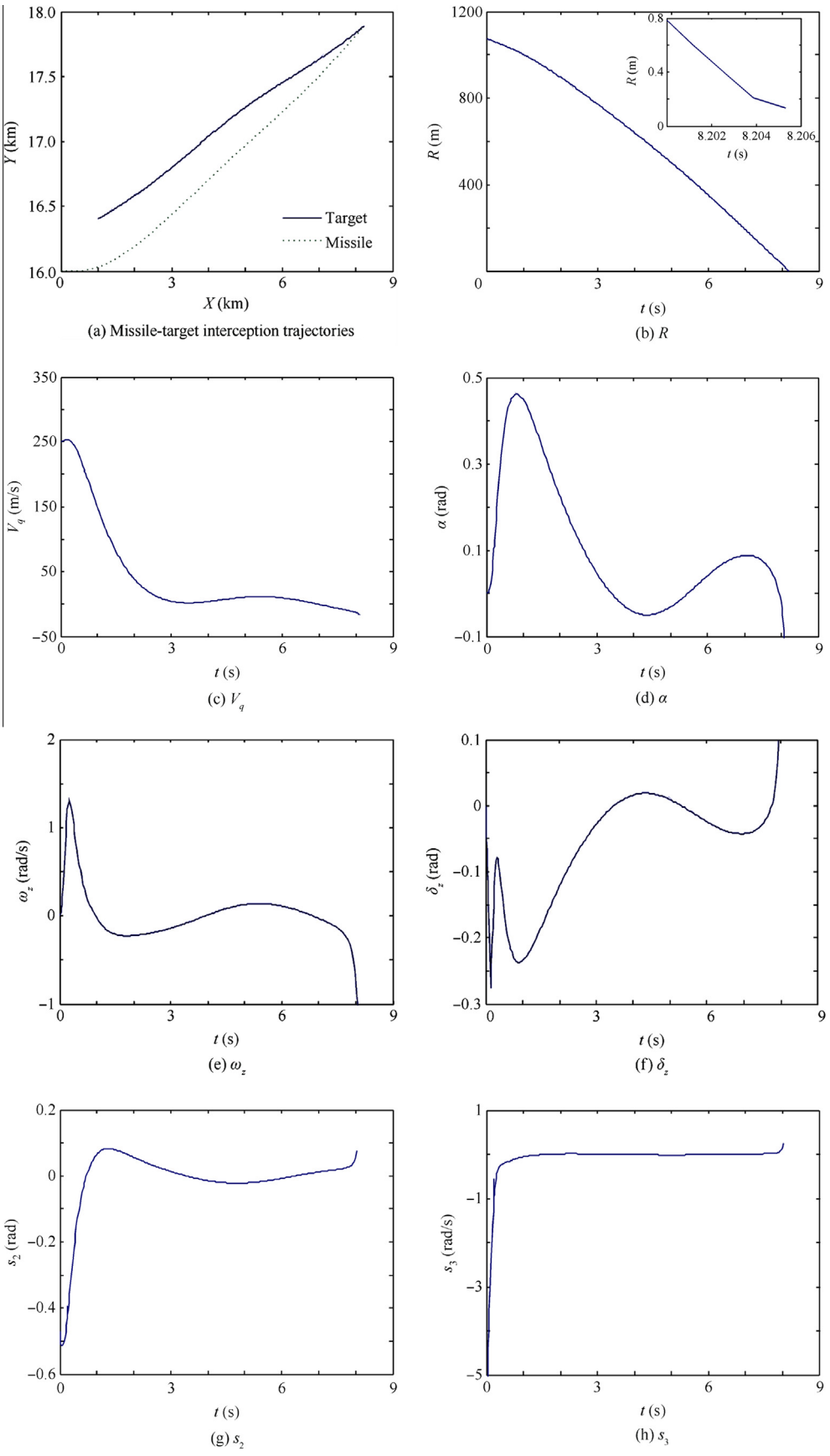

Fig. 3 Simulation results of the proposed IGC law in Case 2.

$$\boldsymbol{P}_1(x_1) = \left[\frac{\mu_{11}}{\sum_{i=1}^{3}\mu_{1i}}, \quad \frac{\mu_{12}}{\sum_{i=1}^{3}\mu_{1i}}, \quad \frac{\mu_{13}}{\sum_{i=1}^{3}\mu_{1i}}\right]^{\mathrm{T}}$$

$$\boldsymbol{P}_2(x_2) = \left[\frac{\mu_{21}}{\sum_{i=1}^{3}\mu_{2i}}, \quad \frac{\mu_{22}}{\sum_{i=1}^{3}\mu_{2i}}, \quad \frac{\mu_{23}}{\sum_{i=1}^{3}\mu_{2i}}\right]^{\mathrm{T}}$$

$$\boldsymbol{P}_3(x_2, x_3) = \left[\frac{\mu_{21}\mu_{31}}{\sum_{i=1}^{3}\mu_{2i}\mu_{3i}}, \quad \frac{\mu_{22}\mu_{32}}{\sum_{i=1}^{3}\mu_{2i}\mu_{3i}}, \quad \frac{\mu_{23}\mu_{33}}{\sum_{i=1}^{3}\mu_{2i}\mu_{3i}}\right]^{\mathrm{T}}$$

where

$$\mu_{11} = \exp\left(-\left(\frac{x_1 + 2\pi}{\pi}\right)^2\right), \quad \mu_{12} = \exp\left(-\left(\frac{x_1 - 2\pi}{\pi}\right)^2\right)$$

$$\mu_{13} = \exp\left(-\left(\frac{x_1}{\pi}\right)^2\right), \mu_{21} = \exp\left(-\left(\frac{x_2 + \pi/2}{\pi/4}\right)^2\right)$$

$$\mu_{22} = \exp\left(-\left(\frac{x_2 - \pi/2}{\pi/4}\right)^2\right), \quad \mu_{23} = \exp\left(-\left(\frac{x_2}{\pi/4}\right)^2\right)$$

$$\mu_{31} = \exp\left(-\left(\frac{x_3 + \pi}{\pi/2}\right)^2\right), \quad \mu_{32} = \exp\left(-\left(\frac{x_3 - \pi}{\pi/2}\right)^2\right)$$

$$\mu_{33} = \exp\left(-\left(\frac{x_3}{\pi/2}\right)^2\right)$$

We evaluate the proposed IGC law in the following two cases:

Case 1: Suppose $d_i = 0$ ($i = 1,2,3$), which means the target does not maneuver and there are no external disturbances.

Case 2: Assume that the target escapes with an acceleration of $a_T = 3g\sin(\pi t/3)$, the missile aerodynamics coefficients vary $+25\%$, and external disturbances $d_2 = 0.1\sin t$ and $d_3 = 0.2\sin t$.

Simulation results of Case 1 and Case 2 are depicted in Figs. 2 and 3, respectively. From Figs. 2(a)–(c) and Figs. 3(a)–(c), we can see that the missile flight trajectories are smooth, the miss distances we get are quite small (0.0749 m and 0.1334 m in Case 1 and Case 2, respectively), and V_q rapidly converges to a small neighborhood of zero. Figs. 2(d)–(e) and Figs. 3(d)–(e) depict the responses of missile dynamics. Figs. 2(f) and 3(f) show the histories of the control deflection. It is observed that the maximum control effort is less than 20°. Finally, histories of the sliding surfaces are shown in Figs. 2(g)–(h) and Figs. 3(g)–(h). The sliding surfaces converge to nearly zero rapidly, which guarantees the interception.

6. Conclusions

(1) With some rational assumptions, the IGC model can be built in a strict-feedback form, and by adopting the backstepping technique, the stability of the entire system states is guaranteed.

(2) The adaptive fuzzy system is effective to approximate the coupling nonlinear functions and the online-adaptive control law is suitable to estimate the unknown parameters in the integrated system.

(3) Simulation results confirm the effectiveness of the proposed method on dealing with missile aerodynamics coefficients varying, target maneuver, and external disturbances.

Acknowledgements

This study was co-supported by the National Natural Science Foundation of China (No. 61074027) and the National Defense Pre-research Foundation of China (No. 9140C48020212HK0101).

References

1. Yan H, Ji HB. Integrated guidance and control for dual-control missiles based on small-gain theorem. *Automatica* 2012;**48**(10):2686–92.
2. Koren A, Idan M, Golan OM. Integrated sliding mode guidance and control for a missile with on–off actuators. *J Guid Control Dyn* 2008;**31**(1):204–14.
3. Williams DE, Richman J, Friedland B. Design of an integrated strapdown guidance and control system for a tactical missile. 1983. Report No. AIAA-1983-2169.
4. Tournes C, Shtessel Y, Rosales A, Fridman L. Phase and gain margins with third order sliding mode control: an integrated guidance application. 2012. Report No. AIAA-2012-4672.
5. Theodoulis S, Gassmann V, Wernert P, Dritsas L, Kitsios I, Tzes A. Guidance and control design for a class of spin-stabilized fin-controlled projectiles. *J Guid Control Dyn* 2013;**36**(2):517–31.
6. Menon PK, Sweriduk GD, Ohlmeyer EJ, Malyevac DS. Integrated guidance and control of moving mass actuated kinetic warheads. *J Guid Control Dyn* 2004;**27**(1):118–26.
7. Kim BS, Calise AJ, Sattigeri RJ. Adaptive, integrated guidance and control design for line-of-sight-based formation flight. *J Guid Control Dyn* 2007;**30**(5):1386–99.
8. Vaddi SS, Menon PK, Ohlmeyer EJ. Numerical state-dependent Riccati equation approach for missile integrated guidance control. *J Guid Control Dyn* 2009;**32**(2):699–703.
9. Xin M, Balakrishnan SN, Ohlmeyer EJ. Integrated guidance and control of missiles with θ-D method. *IEEE Trans Control Syst Technol* 2006;**14**(6):981–92.
10. Shima T, Idan M, Golan OM. Sliding-mode control for integrated missile autopilot guidance. *J Guid Control Dyn* 2006;**29**(2):250–60.
11. Hou MZ, Duan GR. Integrated guidance and control of homing missiles against ground fixed targets. *Chin J Aeronaut* 2008;**21**(2):162–8.
12. Yamasaki T, Balakrishnan SN, Takano H. Separate-channel integrated guidance and autopilot for automatic path-following. *J Guid Control Dyn* 2013;**36**(1):25–34.
13. Dong FY, Lei HM, Zhou CJ, Li J, Shao L. Research of integrated robust high order sliding mode guidance and control for missiles. *Acta Aeronaut Astronaut Sin* 2013;**34**(9):2212–8 [Chinese].
14. Zhao ZH, Shen Y, Li KC, Han YF. An integrated nonlinear guide-control strategy with missile's high order dynamic nature in consideration. *J Astronaut* 2009;**30**(3):1045–51 [Chinese].
15. Stevens BL, Lewis FL. *Aircraft control and simulation*. New York: John Wiley & Sons; 1992, p. 107–116.
16. Sharma M, Richards ND. Adaptive, integrated guidance and control for missile interceptors. 2004. Report No. AIAA-2004-4880.
17. Krstic M, Kanellakopoulos I, Kokotovic P. *Nonlinear and adaptive control design*. New York: John Wiley & Sons; 1995, p. 58–66.
18. Wang LX. *Adaptive fuzzy system and control—design and stability analysis*. Beijing: National Defense Industry Press; 1995, p. 32–3 [Chinese].
19. Wang LX. Stable adaptive fuzzy control of nonlinear systems. *IEEE Trans Fuzzy Syst* 1993;**1**(2):146–55.
20. Shu YJ, Tang S. Integrated guidance and control backstepping design for blended control missile based on NDO. *J Astronaut* 2013;**34**(1):79–85 [Chinese].
21. Zhang BQ, Song SM. Integrated playback design of missile guidance and control based on adaptive sliding-mode control. *J Projectiles Rockets Missiles Guidance* 2009;**29**(5):31–5 [Chinese].

Ran Maopeng is a Ph.D. student in the School of Automation Science and Electrical Engineering at Beihang University. He received his B.S. degree from Beihang University in 2012. His current research interests are missile guidance and control, switch control, and anti-windup.

Wang Qing is a professor and Ph.D. advisor in the School of Automation Science and Electrical Engineering at Beihang University. Her current research interests are missile guidance and control, switch control, and fault detection.

Hou Delong is a Ph.D. student in the School of Automation Science and Electrical Engineering at Beihang University. He received his B.S. degree from Northwestern Polytechnical University in 2009. His current research interest is missile guidance and control.

Dong Chaoyang is a professor and Ph.D. advisor in the School of Aeronautic Science and Engineering at Beihang University. His current research interest is aircraft design.